

# Double-twisted surface spectrum from hybridized Majorana Kramers pairs and wallpaper fermions

Kaito Yoda \* and Ai Yamakage 

Department of Physics, Nagoya University, Nagoya 464-8602, Japan

(Dated: March 13, 2026)

We theoretically investigate the superconducting surface states of wallpaper fermions, which are surface quasiparticles of topological nonsymmorphic crystalline insulators protected by a wallpaper group  $p4g$  symmetry, based on a tight-binding model for the space group  $P4/mbm$  (No. 127). A symmetry-based analysis shows that four types of on-site pair potentials are allowed. Using the symmetries of the wallpaper group  $p4g$  and the one-dimensional topological invariants, we clarify that for the  $A_{1u}$  representation, wallpaper fermions and two Majorana Kramers pairs coexist, and hybridization between them give rise to a *double-twisted* surface state and produces four peaks in the surface density of states. We further find that the mirror Chern number vanishes, indicating that our system realizes mirror-helicity-free surface states. This distinguishes superconducting wallpaper fermions from the other superconducting topological (crystalline) insulators, such as  $\text{Cu}_x\text{Bi}_2\text{Se}_3$  and  $\text{Sn}_{1-x}\text{In}_x\text{Te}$ .

## I. INTRODUCTION

Unconventional superconductors can host gapless Andreev bound states (ABSs) at their boundaries, including chiral, helical, and flat-band edge modes [1–6]. These boundary excitations originate from nontrivial bulk topology of the Bogoliubov–de Gennes (BdG) Hamiltonian and therefore constitute a hallmark of topological superconductivity. Among these gapless boundary states, the self-conjugate ones are regarded as Majorana fermions that obey non-Abelian statistics [7], offering a route toward topological quantum computation [8–11].

The surface physics become richer when superconductivity is realized in topological materials, such as topological insulators [12], topological crystalline insulators [13–17], and topological semimetals [18–22]. For superconducting topological insulators such as  $\text{Cu}_x\text{Bi}_2\text{Se}_3$  [12], mirror-parity-odd pair potentials cannot open a superconducting gap for surface Dirac fermions in the normal states. As a result, in the superconducting states, the Dirac fermions can hybridize with Majorana Kramers pairs, which leads to an anomalous *twisted* surface dispersion distinct from the purely linear spectrum of an isolated Majorana cone [23–26]. A related mechanism has been discussed for superconducting topological crystalline insulators such as  $\text{Sn}_{1-x}\text{In}_x\text{Te}$  [16], where multiple normal-state surface Dirac cones further enrich the superconducting surface spectra. These examples illustrate a general mechanism: gapless surface bands in the normal state can hybridize with superconducting ABSs and generate unconventional surface dispersions, depending on the type of topological surface states in the normal state.

Wallpaper fermions provide a natural unexplored platform in which to test this physics [27–34]. They are surface states of topological nonsymmorphic crystalline

insulators protected by time-reversal symmetry and two orthogonal glide symmetries. Unlike conventional Dirac surface states, wallpaper fermions exhibit fourfold degeneracies enforced by nonsymmorphic symmetry [27]. This feature suggests that hybridized states between wallpaper fermions and superconducting ABSs can give rise to novel quasiparticle states.

In this paper, we theoretically investigate surface states in superconducting wallpaper fermions within a tight-binding model for on-site pair potentials. We first classify the four on-site pairing channels permitted by the crystalline symmetries and identify the  $A_{1u}$  channel as the one in which gapless wallpaper fermions coexist with two Majorana Kramers pairs. For the  $A_{1u}$  pairing channel, we compute the surface spectral function by using the recursive Green’s function method [35]. We find that the hybridization between wallpaper fermions and Majorana Kramers pairs gives rise to *double-twisted* surface spectra and generates four peaks in the surface density of states (DOSs). We further show that these surface spectra are characterized by the absence of mirror helicity that distinguishes them from those of superconducting topological (crystalline) insulators [16, 24].

The paper is organized as follows. In Sec. II, we construct a tight-binding model for the wallpaper fermion systems and classify the on-site pair potentials allowed by the crystalline symmetries. In Sec. III, we analyze the hybridized states for the pairing symmetries in which wallpaper fermions and Majorana Kramers pairs coexist, and discuss the surface DOS. In Sec. IV, we compare our results with previous theoretical studies of superconducting topological insulators [16, 24] by using the mirror Chern number. Finally, Sec. V summarizes this paper.

## II. MODEL

Wallpaper fermions are symmetry-protected surface states that arise in nonsymmorphic crystalline systems with two orthogonal glide symmetries, as realized in the

\* yoda.kaito.c1@s.mail.nagoya-u.ac.jp

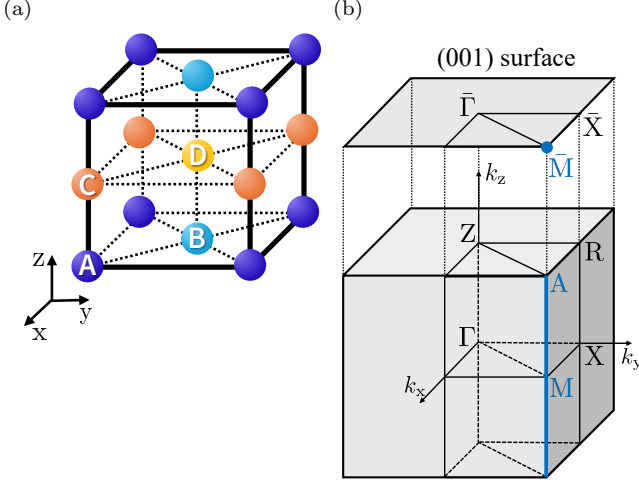


FIG. 1. (Color online) (a) Tetragonal lattice model for wallpaper fermions [27]. (b) Brillouin zone for space group  $P4/mbm$  and (001) surface Brillouin zone [36–39].

wallpaper group  $pgg$  or  $p4g$  [27]. Due to these nonsymorphic symmetries, wallpaper fermions exhibit a fourfold degeneracy at the  $\bar{M}$  point and a twofold degeneracy along the  $\bar{X}\bar{M}$  lines. In this work, we focus on the  $p4g$  case, which possesses higher symmetry than  $pgg$ . In this section, we construct the model of wallpaper fermions for normal and superconducting states.

### A. Tight-binding Hamiltonian for wallpaper fermions

We begin by introducing a tight-binding model for wallpaper fermion systems. We employ the tetragonal lattice model shown in Fig. 1(a), originally proposed in Ref. 27. The crystal structure consists of two types of layers stacked along the  $z$  axis: one layer contains the A and B sublattices, while the other contains the C and D sublattices. The bulk crystal symmetry is described by the space group  $P4/mbm$  (No. 127). The (001) surface preserves the symmetries of the wallpaper group  $p4g$ . The bulk and surface Brillouin zones are shown in Fig. 1(b). This model has three internal degrees of freedom: spin ( $\uparrow$  and  $\downarrow$ ), layer sublattice [A(B) and C(D)], and in-plane sublattice [A(C) and B(D)]. These are represented by Pauli matrices  $s_\nu$ ,  $\rho_\nu$ , and  $\sigma_\nu$  ( $\nu = 0, x, y, z$ ), respectively. Hereafter, we set the lattice constants to unity.

We now construct a tight-binding Hamiltonian  $H_{\text{wp}}(\mathbf{k})$  consistent with the space group  $P4/mbm$ . For each symmetry operation  $g$  in the space group  $P4/mbm$ , the Hamiltonian satisfies  $D_{\mathbf{k}}(g)H_{\text{wp}}(\mathbf{k})D_{\mathbf{k}}(g)^\dagger = H_{\text{wp}}(g\mathbf{k})$ , where  $D_{\mathbf{k}}(g)$  is the representation matrix of  $g$  at momentum  $\mathbf{k}$ . The representations of generators for this lattice system are derived as follows (see Appendix A) [40]:

$$D_{\mathbf{k}}(\{4_{001}^+|\mathbf{0}\}) = \frac{1}{\sqrt{2}}(s_0 - is_z)\rho_0\sigma_0, \quad (1)$$

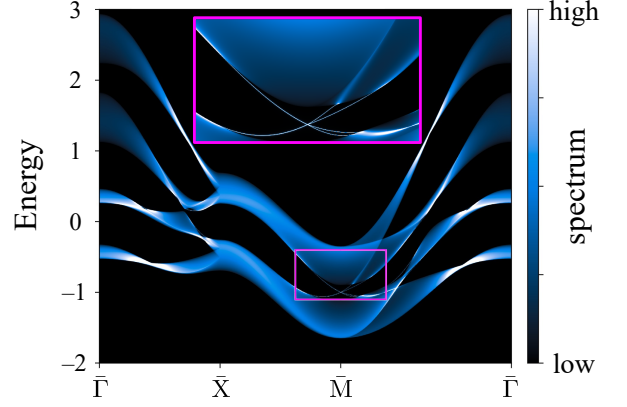


FIG. 2. (Color online) Surface energy spectrum for a semi-infinite system with the (001) surface on the C–D layers. The inset shows an enlarged view near the  $\bar{M}$  point. A fourfold degeneracy at the  $\bar{M}$  point and a twofold degeneracy along the  $\bar{X}\bar{M}$  line are confirmed. The parameters are fixed as  $t_1 = 1$ ,  $v_{r1} = 0.25$ ,  $v_{s1} = 0.2$ ,  $t_2 = 0.5$ ,  $v_{s2} = -0.2$ ,  $v'_{s2} = 0.15$ ,  $u_1 = 0.3$ ,  $u_2 = -0.45$ ,  $w_1 = 0.2$ ,  $w_2 = 0.05$ ,  $w_3 = 0.05$ ,  $w_4 = -0.02$ ,  $w_5 = 0.11$ ,  $w_6 = -0.08$ ,  $v_1 = 0.2$ ,  $v_2 = 0.1$ ,  $p_1 = 0$ ,  $p_2 = 0.3$ .

$$D_{\mathbf{k}}(\{2_{100}|1/2\ 1/2\ 0\}) = -ie^{-i\frac{k_x - k_y}{2}} s_x \rho_x \sigma_x, \quad (2)$$

$$D_{\mathbf{k}}(\{I|\mathbf{0}\}) = s_0 \rho_x \sigma_0. \quad (3)$$

The time-reversal symmetry imposes  $\Theta H_{\text{wp}}(\mathbf{k})\Theta^{-1} = H_{\text{wp}}(-\mathbf{k})$ , with  $\Theta = -is_y\mathcal{K}$  and  $\mathcal{K}$  denotes complex conjugation. For in-plane directions, we include the nearest-neighbor hopping

$$\begin{aligned} H_{\parallel}^{(1)}(\mathbf{k}) := & t_1 \cos \frac{k_x}{2} \cos \frac{k_y}{2} [s_0 \rho_0 \sigma_x] \\ & + v_{r1} \cos \frac{k_x}{2} \cos \frac{k_y}{2} [s_y \rho_0 \sigma_y] \\ & + v_{s1} \sin \frac{k_x}{2} \cos \frac{k_y}{2} [s_y \rho_z \sigma_x] \\ & - v_{s1} \cos \frac{k_x}{2} \sin \frac{k_y}{2} [s_x \rho_z \sigma_x], \end{aligned} \quad (4)$$

and the next-nearest-neighbor hopping

$$\begin{aligned} H_{\parallel}^{(2)}(\mathbf{k}) := & t_2 (\cos k_x + \cos k_y) [s_0 \rho_0 \sigma_0] \\ & + v_{s2} \left( \sin k_x [s_x \rho_z \sigma_z] + \sin k_y [s_y \rho_z \sigma_z] \right) \\ & + v'_{s2} \left( \sin k_x [s_y \rho_z \sigma_0] - \sin k_y [s_x \rho_z \sigma_0] \right). \end{aligned} \quad (5)$$

For out-of-plane directions, we include the nearest-neighbor hopping

$$H_{\perp}^{(1)}(\mathbf{k}) := u_1 \cos \frac{k_z}{2} [s_0 \rho_x \sigma_0] + u_2 \sin \frac{k_z}{2} [s_0 \rho_y \sigma_0], \quad (6)$$

the next-nearest-neighbor hopping

$$H_{\perp}^{(2)}(\mathbf{k}) := w_1 \cos \frac{k_x}{2} \cos \frac{k_y}{2} \cos \frac{k_z}{2} [s_0 \rho_x \sigma_x]$$

$$\begin{aligned}
& + w_2 \cos \frac{k_x}{2} \cos \frac{k_y}{2} \cos \frac{k_z}{2} [s_z \rho_x \sigma_y] \\
& + w_3 \cos \frac{k_x}{2} \cos \frac{k_y}{2} \sin \frac{k_z}{2} [s_0 \rho_y \sigma_x] \\
& + w_4 \cos \frac{k_x}{2} \cos \frac{k_y}{2} \sin \frac{k_z}{2} [s_z \rho_y \sigma_y] \\
& + w_5 \cos \frac{k_x}{2} \sin \frac{k_y}{2} \sin \frac{k_z}{2} [s_y \rho_x \sigma_y] \\
& + w_5 \sin \frac{k_x}{2} \cos \frac{k_y}{2} \sin \frac{k_z}{2} [s_x \rho_x \sigma_y] \\
& + w_6 \sin \frac{k_x}{2} \cos \frac{k_y}{2} \cos \frac{k_z}{2} [s_x \rho_y \sigma_y] \\
& + w_6 \cos \frac{k_x}{2} \sin \frac{k_y}{2} \cos \frac{k_z}{2} [s_y \rho_y \sigma_y], \quad (7)
\end{aligned}$$

and the next-next-nearest-neighbor hopping

$$\begin{aligned}
H_{\perp}^{(3)}(\mathbf{k}) & := v_1 (\cos k_x + \cos k_y) \cos \frac{k_z}{2} [s_0 \rho_x \sigma_0] \\
& + v_2 (\cos k_x + \cos k_y) \sin \frac{k_z}{2} [s_0 \rho_y \sigma_0], \quad (8)
\end{aligned}$$

in addition to the intra-sublattice hopping

$$H_{\perp}^{(4)}(\mathbf{k}) := p_1 \cos k_z [s_0 \rho_0 \sigma_0] + p_2 \sin k_z [s_z \rho_z \sigma_z]. \quad (9)$$

Here, we take the basis as  $(c_{X,\uparrow}, c_{X,\downarrow})$  ( $X = A, B, C, D$ ). The tight-binding Hamiltonian is then given by

$$\begin{aligned}
H_{\text{wp}}(\mathbf{k}) & := H_{\parallel}^{(1)}(\mathbf{k}) + H_{\parallel}^{(2)}(\mathbf{k}) \\
& + H_{\perp}^{(1)}(\mathbf{k}) + H_{\perp}^{(2)}(\mathbf{k}) + H_{\perp}^{(3)}(\mathbf{k}) + H_{\perp}^{(4)}(\mathbf{k}). \quad (10)
\end{aligned}$$

Figure 2 shows the surface energy spectrum of a semi-infinite system with a (001) surface in the C–D layer. The surface spectrum is computed using the recursive Green's function method [35]. We confirm the characteristic wallpaper fermion surface states, and thus adopt  $H_{\text{wp}}(\mathbf{k})$  as a normal Hamiltonian throughout this work [41].

### B. Classification of pair potentials

To describe the superconducting states, we define the BdG Hamiltonian as

$$H_{\text{scwp}}(\mathbf{k}) := [H_{\text{wp}}(\mathbf{k}) - \mu] \tau_z + \hat{\Delta}_i \tau_x, \quad (11)$$

where  $\mu$  is the chemical potential and  $\hat{\Delta}_i$  denotes the pair potential. Here,  $\tau_{\nu}$  ( $\nu = 0, x, y, z$ ) are Pauli matrices in the Nambu (particle–hole) space. We take the Nambu basis as  $(c_{X,\uparrow}, c_{X,\downarrow}, c_{X,\downarrow}^{\dagger}, -c_{X,\uparrow}^{\dagger})$ .

Pair potentials are decomposed into irreducible representations (irreps) of the point group  $D_{4h}$ , which is the rotational part of space group  $P4/mbm$ . Restricting on-site pairings in this work, and imposing Fermi–Dirac statistics:  $s_y \hat{\Delta}_i^{\dagger} s_y = \hat{\Delta}_i$ , we identify four symmetry-distinct on-site pair potentials,  $\hat{\Delta}_1$ – $\hat{\Delta}_4$ , listed in Table I.

TABLE I. Characters of the point group  $D_{4h}$  and the corresponding on-site pair potentials. We impose Fermi–Dirac statistics:  $s_y \hat{\Delta}_i^{\dagger} s_y = \hat{\Delta}_i$ .  $\Delta_0$  is a momentum-independent constant.

Irrep	$2C_4$	$2C'_2$	$I$	Basis	Pair potential
$A_{1g}$	1	1	1	$k_x^2 + k_y^2, k_z^2$	$\hat{\Delta}_1 := \Delta_0 s_0 \rho_0 \sigma_0$
$A_{2g}$	1	–1	1	$k_x k_y (k_x^2 - k_y^2)$	$\hat{\Delta}_2 := \Delta_0 s_0 \rho_0 \sigma_z$
$A_{1u}$	1	1	–1	$k_x k_y k_z (k_x^2 - k_y^2)$	$\hat{\Delta}_3 := \Delta_0 s_0 \rho_z \sigma_z$
$A_{2u}$	1	–1	–1	$k_z$	$\hat{\Delta}_4 := \Delta_0 s_0 \rho_z \sigma_0$

TABLE II. Compatibility relations between the irreps of the bulk point group  $D_{4h}$  and surface point group  $C_{4v}$ . The right-most column summarizes the superconducting gap structure in surface wallpaper fermions reported in Ref. 34.

Irrep of $D_{4h}$	Irrep of $C_{4v}$	Gap structure
$A_{1g}$ ( $\hat{\Delta}_1$ )	$A_1$	Fully gapped
$A_{2u}$ ( $\hat{\Delta}_4$ )		
$A_{2g}$ ( $\hat{\Delta}_2$ )	$A_2$	Point nodes along the $\bar{\Gamma}\bar{M}$ line
$A_{1u}$ ( $\hat{\Delta}_3$ )		

## III. SURFACE STATES

In this section, we analyze the (001) surface states for each pairing symmetry based on symmetry-based and numerical approaches.

### A. Wallpaper fermions in superconducting states

To observe hybridization between the wallpaper fermions and Majorana Kramers pairs, the wallpaper fermions need to remain gapless in the superconducting state. Within the weak-coupling assumption, whether a given pairing opens a gap on the surface dispersion is determined solely by surface symmetry, i.e., the compatibility of irreps of energy bands in the normal state and pair potential in the superconducting state. As shown in Ref. 34, we previously reported the superconducting gap structures in wallpaper fermions based on the  $p4g$  surface symmetries. Pair potentials belonging to the  $A_2$  representation of the point group  $C_{4v}$ , the rotational part of the wallpaper group  $p4g$ , exhibit symmetry-enforced point nodes along the  $\bar{\Gamma}\bar{M}$  lines, whereas those belonging to the  $A_1$  representation are fully gapped. Using compatibility relations between the bulk point group  $D_{4h}$  and the surface point group  $C_{4v}$  in Table II, we therefore conclude that the  $\Delta_2$  and  $\Delta_3$  pairings do not open a superconducting gap in the wallpaper fermion dispersion along the  $\bar{\Gamma}\bar{M}$  lines.

## B. Majorana Kramers pairs in wallpaper fermion systems

Next, we discuss the emergence of Majorana Kramers pairs for the  $\Delta_2$  and  $\Delta_3$  pairings at the  $\bar{M}$  point. Majorana Kramers pairs appear at the  $\bar{M}$  point when the BdG Hamiltonian along the MA line,  $(k_x, k_y) = (\pi, \pi)$ ,  $-\pi \leq k_z \leq \pi$  [Fig. 1(b)], is topologically nontrivial. The BdG Hamiltonian (11) possesses a chiral symmetry:  $\Gamma H_{\text{scwp}}(\mathbf{k})\Gamma^\dagger = -H_{\text{scwp}}(\mathbf{k})$  ( $\Gamma := \tau_y$ ) and thus one may define a winding number [42]. However, we consider a time-reversal-invariant one-dimensional (1D) path, on which the conventional winding number is forced to vanish due to time-reversal symmetry [43]. We therefore exploit order-two crystalline symmetries that leave the MA line invariant [44].

The MA line is invariant under twofold rotation about the  $z$  axis,  $C_{2z} := \{2_{001}|\mathbf{0}\}$ , whose representation satisfies  $D_{\mathbf{k}}(C_{2z})^2 = -1$ . Moreover, the pair potentials  $\hat{\Delta}_2$  and  $\hat{\Delta}_3$  are even under  $C_{2z}$ . Following the criterion derived in Refs. 43 and 44, we can then define a  $\mathbb{Z}$  topological invariant, the magnetic winding number,

$$W[C_{2z}] := \frac{i}{4\pi} \int_{-\pi}^{\pi} dk_z \text{Tr} \left[ \Gamma[C_{2z}] H_{\text{scwp}}^{-1}(\mathbf{k}) \frac{\partial H_{\text{scwp}}(\mathbf{k})}{\partial k_z} \right], \quad (12)$$

where  $\Gamma[C_{2z}] := i(D_{\mathbf{k}}(C_{2z})\tau_0)\Gamma$  is the magnetic chiral operator. Here,  $D_{\mathbf{k}}(C_{2z})\tau_0$  denotes the representation of  $C_{2z}$  for the BdG Hamiltonian (11).

We now evaluate Eq. (12) for the BdG Hamiltonian (11) with  $\Delta_2$  and  $\Delta_3$  pairing. First of all, along the MA line in the space group  $P4/mbm$ , the magnetic winding number is restricted to  $4\mathbb{Z} \in \{0, \pm 4, \pm 8, \dots\}$  because of four dimensional irreps at the  $\bar{M}$  point in the wallpaper group  $p4g$  [36–38, 45, 46]. In addition, a set of necessary conditions for the magnetic winding number to take a nonzero value, formulated in terms of additional order-two crystalline symmetries, has been derived in Ref. 43. Based on these conditions, we find that  $W[C_{2z}]$  always vanishes for even-parity pairings under inversion [47], and the BdG Hamiltonian along the MA line is topologically trivial for  $\Delta_2$  pairings. In contrast, for  $\Delta_3$  pairing,  $W[C_{2z}]$  can be nonzero. Hence, combining the results of Sec. III A and the above analysis, we conclude that only for the  $\Delta_3$  pairing, the gapless wallpaper fermions and the Majorana Kramers pairs can coexist along the  $\bar{\Gamma}\bar{M}$  line.

## C. Hybridized state

In this subsection, we analyze the superconducting surface states along the  $\bar{\Gamma}\bar{M}\bar{\Gamma}$  line for the  $\Delta_3$  pairing. The parameters of the tight-binding Hamiltonian (10) are the same as those written in Fig. 2. We set the chemical potential to  $\mu = -0.75$  so that the Fermi level crosses the bulk spectra at the  $\bar{M}$  point [Fig. 3(a)], and fix the pairing amplitude to  $\Delta_0 = 0.02$ , assuming weak-coupling

pairing. For this parameter set, we obtain  $W[C_{2z}] = 4$ , and hence double Majorana Kramers pairs appear at the  $\bar{M}$  point.

The resulting surface spectrum for the  $\Delta_3$  pairing is shown in Fig. 3(b). The wallpaper fermion branches that cross the Fermi level in the normal state remain gapless for  $k_{\parallel}/\pi \sim 0.8$  (1.2) and 0.9 (1.1) in the superconducting state, consistent with the symmetry-enforced point nodes along the  $\bar{\Gamma}\bar{M}$  line. In addition, double Majorana Kramers pairs emerge at the  $\bar{M}$  point, as expected from the nontrivial magnetic winding number  $W[C_{2z}] = 4$ . A salient feature is the presence of two types of hybridization: (i) between wallpaper fermions themselves for  $0.8$  (1.1)  $< k_{\parallel}/\pi < 0.9$  (1.2) and (ii) between wallpaper fermions and Majorana Kramers pairs for  $0.9 < k_{\parallel}/\pi < 1.1$ . As a consequence, the surface spectrum exhibits a characteristic *double-twisted* structure along the  $\bar{\Gamma}\bar{M}$  line. Such a spectral reconstruction is absent in conventional time-reversal-invariant topological superconductivity where the low-energy surface state is solely composed of Majorana Kramers pairs. The key ingredient is the persistence of crystalline-symmetry-protected wallpaper fermions in the superconducting state, which provides additional gapless channels that can hybridize with Majorana Kramers pairs. Appendix B summarizes the numerical results and theoretical discussions for the superconducting surface states for the other pairings.

We further compute the surface DOS per unit area [Fig. 3(c)] and compare it with the bulk DOS per unit volume [Fig. 3(d)]. The *double-twisted* dispersion yields a nearly flat segment in the surface spectrum [Fig. 3(b)], leading to a weak enhancement in the surface DOS around  $E/\Delta_0 \simeq \pm 0.066$  and sharp peaks around  $E/\Delta_0 \simeq \pm 0.294$ . In the same energy window of these sharp peaks, the bulk DOS is also enhanced, indicating that the bulk states contribute to the spectral weight. Nevertheless, the bulk DOS does not exhibit comparably sharp peaks. This contrast suggests that the pronounced surface DOS peaks at  $E/\Delta_0 \simeq \pm 0.294$  originate from combined surface and bulk contributions, and the surface component is comparable in magnitude to the bulk one.

## IV. DISCUSSION

In this section, we clarify how the superconducting surface state of wallpaper fermions discussed in Sec. III differs from those of a superconducting topological insulator  $\text{Cu}_x\text{Bi}_2\text{Se}_3$  [24] and a superconducting topological crystalline insulator  $\text{Sn}_{1-x}\text{In}_x\text{Te}$  [16]. Their surface spectra can be examined along a mirror-invariant line, where the energy eigenstates can be decomposed into mirror eigenspaces. This enables a characterization in terms of mirror Chern number [24, 48], and allows us to point out what is unique to the wallpaper fermion case.

We briefly summarize the general properties of the mirror Chern number  $n_{\mathcal{M}}$  based on Ref. 24. Let  $n_{+i}$  and  $n_{-i}$  denote the Chern numbers evaluated in the

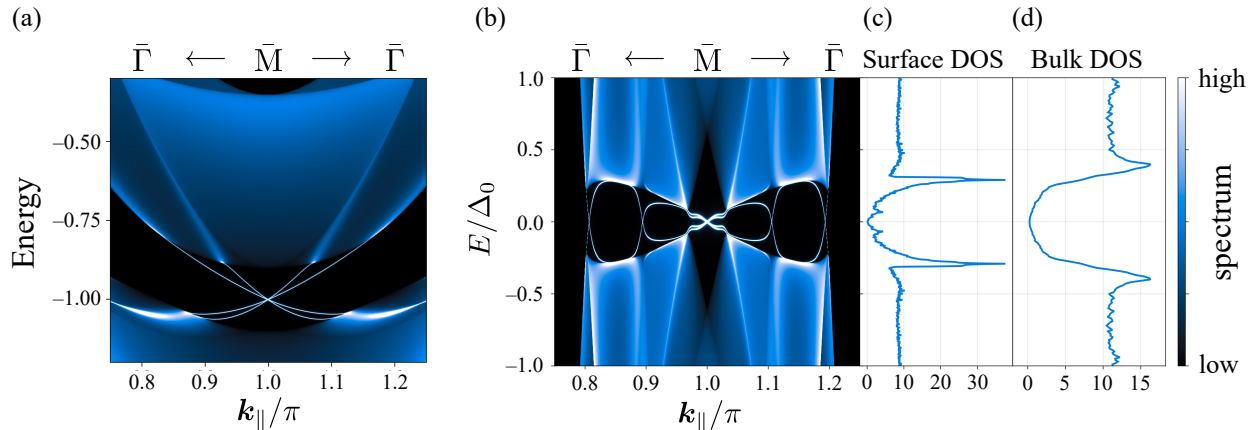


FIG. 3. (Color online) Surface spectral function for a (001) surface on the C–D layer along the  $\bar{\Gamma}\bar{M}\bar{\Gamma}$  line in (a) the normal state and (b) the superconducting state with  $\Delta_3$  pairing ( $\Delta_0 = 0.02, \mu = -0.75$ ). (c) Surface and (d) bulk density of states for the  $\Delta_3$  pairing.

$+i$  and  $-i$  mirror eigensectors, respectively. The mirror Chern number is defined as  $n_{\mathcal{M}} := (n_{+i} - n_{-i})/2$ . For a time-reversal-invariant system, time reversal exchanges the two mirror sectors, enforcing  $n_{+i} = -n_{-i}$ , and hence  $n_{\mathcal{M}} = n_{+i} = -n_{-i}$ . The magnitude  $|n_{\mathcal{M}}|$  gives the number of mirror-helical edge modes on a mirror-invariant boundary. In addition, the sign  $\eta := \text{sgn}(n_{\mathcal{M}}) = \text{sgn}(n_{+i}) = -\text{sgn}(n_{-i})$  specifies the mirror helicity: in our convention, for  $\eta > 0$  ( $\eta < 0$ ), the  $+i$  ( $-i$ ) sector hosts right-going modes on the mirror-invariant line.

Figures 4(a) and 4(b) schematically illustrate the surface states of a topological insulator and its superconducting state [24], while Figs. 4(c) and 4(d) illustrate those of a topological crystalline insulator and its superconducting state [16]. For the superconducting topological insulators [Fig. 4(b)], the surface spectrum on the mirror line hosts a single helical pair with positive mirror helicity in our convention, corresponding to  $n_{\mathcal{M}} = +1$ . Similarly, the superconducting topological crystalline insulator [Fig. 4(d)] exhibits two helical pairs with positive mirror helicity, corresponding to  $n_{\mathcal{M}} = +2$ . In both cases, the direction of propagation is locked to the mirror eigenvalue; the surface states are therefore characterized by a nonzero mirror Chern number and a well-defined mirror helicity.

In contrast, the superconducting wallpaper fermion behaves qualitatively differently. In Sec. III C, we focused on the  $\bar{\Gamma}\bar{M}\bar{\Gamma}$  line, which is invariant under the mirror operation  $\{m_{1\bar{1}0}|1/2\ 1/2\ 0\}$ . Consequently, the normal state spectrum [Fig. 3(a)] and the superconducting spectrum [Fig. 3(b)] can be resolved into the  $+i$  and  $-i$  sectors as shown in Figs. 5(a) and 5(b) and Figs. 5(c) and 5(d), respectively. From Figs. 5(c) and 5(d), each mirror eigensector contains both right- and left-going branches along  $\bar{\Gamma}\bar{M}\bar{\Gamma}$  lines. Therefore, the propagation direction is not locked to the mirror eigenvalue, which implies that the net Chern number within each sector cancels, result-

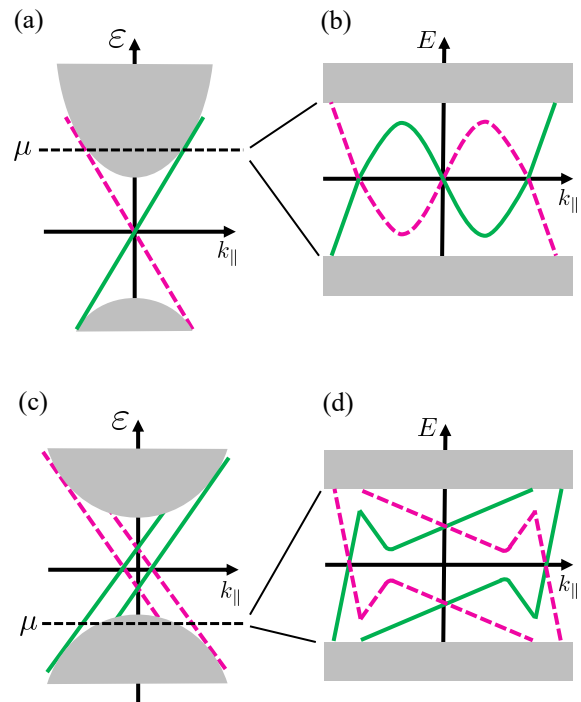


FIG. 4. (Color online) Schematic surface dispersions for (a) a topological insulator, (b) its superconducting state, (c) a topological crystalline insulator, and (d) its superconducting state. Solid green (dotted magenta) lines indicate the dispersions belonging to  $+i$  ( $-i$ ) mirror eigenspace.

ing in  $n_{\mathcal{M}} = n_{+i} = n_{-i} = 0$ . Equivalently, the surface spectrum is mirror-helicity-free in the sense that the mirror eigenvalue does not uniquely determine the direction of motion.

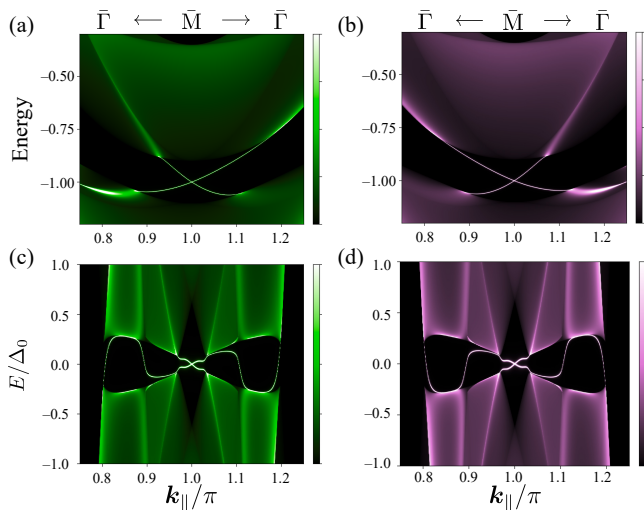


FIG. 5. (Color online) Energy spectra along the  $\bar{\Gamma}\bar{M}\bar{\Gamma}$  line, resolved into mirror eigensectors. Normal state spectra in the (a)  $+i$  and (b)  $-i$  sectors. Superconducting state spectra for the  $\Delta_3$  pairing in the (c)  $+i$  and (d)  $-i$  sectors.

## V. CONCLUSION

In this work, we constructed a symmetry-consistent tight-binding model and investigated the (001) surface states in superconducting wallpaper fermions. Based on a symmetry-based theoretical analysis, we classified four types of on-site pairings allowed by  $D_{4h}$  symmetry, and found that the  $\Delta_3$  pairing supports both gapless wallpaper fermions and double Majorana Kramers pairs along the  $\bar{\Gamma}\bar{M}$  lines. In this pairing, hybridization between these quasiparticles yields a characteristic *double-twisted* surface spectrum. In addition, surface DOS has peak structures, reflecting the interplay between symmetry-protected wallpaper fermions and Majorana Kramers pairs. We further showed that the resulting surface spectrum is mirror-helicity-free, in sharp contrast to a superconducting topological insulator  $\text{Cu}_x\text{Bi}_2\text{Se}_3$  and a superconducting topological crystalline insulator  $\text{Sn}_{1-x}\text{In}_x\text{Te}$ , which are characterized by a nonzero mirror Chern number. These findings help to elucidate and explore the non-trivial nature of topological superconductivity in topological materials.

## ACKNOWLEDGMENTS

This work is supported by JSPS KAKENHI for Grants (Grants Nos. JP24H00853 and JP25K07224).

### Appendix A: Representation matrices

In this section, we briefly describe the derivation of the representation matrices  $D_{\mathbf{k}}(g)$  in Eqs. (1)–(3). We

use the Fourier transformation of the real-space fermion operators,

$$c_{\mathbf{k},s,X}^\dagger := \frac{1}{\sqrt{N}} \sum_{\mathbf{n}} e^{i\mathbf{k}\cdot(\mathbf{n}+\boldsymbol{\tau}_X)} c_{s,\mathbf{n}+\boldsymbol{\tau}_X}^\dagger, \quad (\text{A1})$$

where  $s = \uparrow, \downarrow$ ,  $X = \text{A, B, C, D}$ . Here,  $\mathbf{n}$  denotes a lattice vector,  $N$  is the number of unit cells, and  $\boldsymbol{\tau}_X$  specifies the position of sublattice  $X$  from  $\mathbf{n}$ . In this convention, for a space group operation  $g = \{p_g|\mathbf{a}_g\}$ , the representation matrix can be decomposed into spin, sublattice (SL), and phase factor parts as [40]

$$[D_{\mathbf{k}}(g)]_{s'X',sX} = [D^{(\text{spin})}(p_g)]_{s',s} [D^{(\text{SL})}(g)]_{X',X} e^{-i(p_g\mathbf{k})\cdot\mathbf{a}_g}. \quad (\text{A2})$$

Here,  $D^{(\text{spin})}(p_g)$  describes the action of the point group part  $p_g$  on the spin sector, while  $D^{(\text{SL})}(g)$  is the permutation matrix representing sublattice transformation.

For the generators considered in the main text, the spin part is given by

$$D^{(\text{spin})}(\{4_{001}^+|\mathbf{0}\}) = \exp\left(-i\frac{\pi}{4}s_z\right) = \frac{1}{\sqrt{2}}(s_0 - is_z), \quad (\text{A3})$$

$$D^{(\text{spin})}(\{2_{100}|\mathbf{0}\}) = \exp\left(-i\frac{\pi}{2}s_x\right) = -is_x, \quad (\text{A4})$$

$$D^{(\text{spin})}(\{I|\mathbf{0}\}) = s_0. \quad (\text{A5})$$

Using the sublattice basis (A, B, C, D), the permutation matrix is derived as

$$D^{(\text{SL})}(\{4_{001}^+|\mathbf{0}\}) = \rho_0\sigma_0, \quad (\text{A6})$$

$$D^{(\text{SL})}(\{2_{100}|1/2\ 1/2\ 0\}) = \rho_x\sigma_x, \quad (\text{A7})$$

$$D^{(\text{SL})}(\{I|\mathbf{0}\}) = \rho_x\sigma_0. \quad (\text{A8})$$

Finally, by evaluating the phase factor  $e^{-i(p_g\mathbf{k})\cdot\mathbf{a}_g}$  for each generator, we obtain the explicit forms of  $D_{\mathbf{k}}(g)$  given in Eqs. (1)–(3).

## Appendix B: Surface states for the other pair potentials

In this section, we summarize the superconducting surface states for four symmetry-distinct pair potentials.

### 1. Comparison with surface states for each pair potential

As shown in Fig. 6(a), for the  $\Delta_1$  pairing, which corresponds to  $s$ -wave superconductivity, both bulk states and wallpaper fermions are fully gapped. For the  $\Delta_2$  pairing [Fig. 6(b)], symmetry-protected line nodes exist on the bulk (110) plane, and therefore no superconducting gap opens in the bulk spectrum along the  $\bar{\Gamma}\bar{M}$  direction. In addition, we confirm that Majorana Kramers pairs protected by  $W[C_{2z}]$  do not appear. In contrast, for the  $\Delta_4$

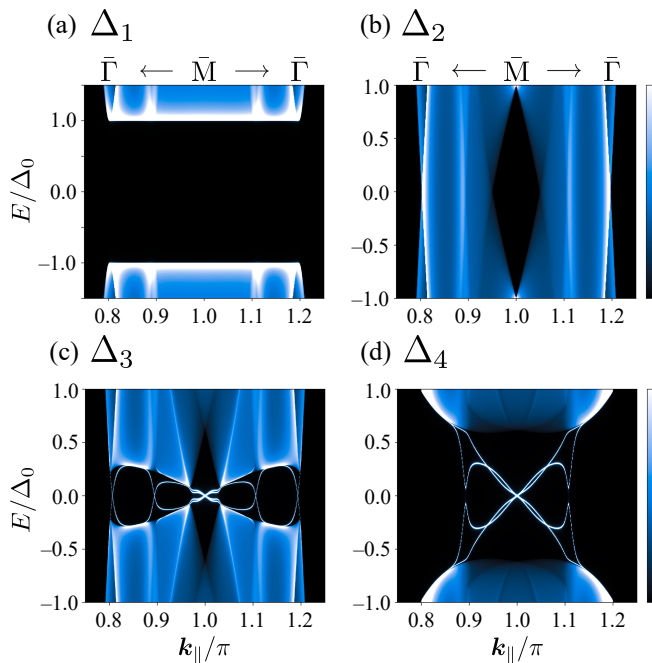


FIG. 6. (Color online) Superconducting surface states along the  $\bar{\Gamma}\bar{M}\bar{\Gamma}$  line for (a)  $\Delta_1$ , (b)  $\Delta_2$ , (c)  $\Delta_3$ , and (d)  $\Delta_4$  pairings. The parameters are the same as those used in Sec. III C.

pairings [Fig. 6(d)], a superconducting gap opens in both the bulk and surface states, and Majorana Kramers pairs emerge at the  $\bar{M}$  point (see Appendix B 2). From these results, we find that hybridization between double Majorana Kramers pairs and wallpaper fermions occurs only for the  $\Delta_3$  pairing.

## 2. Topological nature for the $\Delta_4$ pairing

In this subsection, we discuss that the  $\Delta_4$  pairing has the  $\mathbb{Z}_2$  topological invariant, applying the criterion derived in Ref. 44. We consider the glide with respect to the  $yz$  plane

$$M_x := \{m_{100}|1/2 \ 1/2 \ 0\}, \quad (\text{B1})$$

which is an order-two symmetry that leaves the MA ( $k_x = k_y = \pi$ ) line invariant. The above operation is squared to be  $M_x^2 = \{^dE|0 \ 1 \ 0\}$ , where  $^dE$  denotes the “ $2\pi$  rotation” in the double group, hence

$$D_{\mathbf{k}}(M_x^2) = D_{M_x\mathbf{k}}(M_x)D_{\mathbf{k}}(M_x) = 1, \quad (\text{B2})$$

on the MA line. Choosing the gauge as  $H_{\text{wp}}(\mathbf{k}) = H_{\text{wp}}(\mathbf{k} + \mathbf{G})$  with  $\mathbf{G}$  a reciprocal lattice vector,  $D_{M_x\mathbf{k}}(M_x) = D_{\mathbf{k}}(M_x)$  on the MA line, the above relation reduces to

$$D_{\mathbf{k}}(M_x)^2 = 1. \quad (\text{B3})$$

The pair potential is even parity for the glide,

$$D_{\mathbf{k}}(M_x)\hat{\Delta}_4D_{\mathbf{k}}(M_x)^\dagger = +\hat{\Delta}_4. \quad (\text{B4})$$

The above two relations corresponds to the type D (non-symmorphic) in Table II in Ref. 44.

The other surface symmetry operation  $M_y := \{m_{010}|1/2 \ 1/2 \ 0\}$  anticommutes with  $M_x$ ,  $\{M_x, M_y\} = 0$ . The  $\Delta_4$  pairing is odd parity for the inversion. Applying the Fermi-surface criterion summarized in Fig. 5 of Ref. 44, one finds that a  $\mathbb{Z}_2$  topological invariant  $\nu_{\pm}[M_x]$  can be defined in each eigenspace of  $M_x$  and in the weak-coupling limit, these invariants are given by

$$\nu_{\pm}[M_x] = \frac{N_{\text{occ}}(\pi) - N_{\text{occ}}(0)}{4} \pmod{2}, \quad (\text{B5})$$

where  $N_{\text{occ}}(k_z)$  denotes the number of occupied bands at momentum  $k_z$  in the normal state.

In our case, the bulk bands at the M and A point are necessarily fourfold degenerate, owing to four dimensional irreps in the space group  $P4/mbm$  [36–38, 45, 46]. Therefore, if a Fermi surface exists along the MA line, we obtain  $\nu_+[M_x] = \nu_-[M_x] = 1$ , implying a Majorana Kramers pair in each eigenspace. Hence, for the  $\Delta_4$  pairing, double Majorana Kramers pairs appear at the  $\bar{M}$  point, as shown in Fig. 6(d). The above discussion also applies upon exchanging  $M_x$  and  $M_y$ . Therefore, we can similarly define  $\nu_{\pm}[M_y]$ . However, it is not independent of  $\nu_{\pm}[M_x]$  owing to  $[M_x, M_y] \neq 0$ .

[1] X.-L. Qi and S.-C. Zhang, Topological insulators and superconductors, *Rev. Mod. Phys.* **83**, 1057 (2011).  
[2] T. Mizushima, Y. Tsutsumi, T. Kawakami, M. Sato, M. Ichioka, and K. Machida, Symmetry-Protected Topological Superfluids and Superconductors —From the Basics to  $^3\text{He}$ —, *J. Phys. Soc. Jpn.* **85**, 022001 (2016).  
[3] M. Sato and S. Fujimoto, Majorana Fermions and Topology in Superconductors, *J. Phys. Soc. Jpn.* **85**, 072001 (2016).  
[4] C.-K. Chiu, J. C. Y. Teo, A. P. Schnyder, and S. Ryu, Classification of topological quantum matter with symmetries, *Rev. Mod. Phys.* **88**, 035005 (2016).

[5] M. Sato and Y. Ando, Topological superconductors: a review, *Rep. Prog. Phys.* **80**, 076501 (2017).  
[6] R. Aguado, Majorana quasiparticles in condensed matter, *Riv. Nuovo Cim.* **40**, 523 (2017).  
[7] D. A. Ivanov, Non-Abelian Statistics of Half-Quantum Vortices in  $p$ -Wave Superconductors, *Phys. Rev. Lett.* **86**, 268 (2001).  
[8] A. Kitaev, Anyons in an exactly solved model and beyond, *Ann. Phys.* **321**, 2 (2006).  
[9] C. Nayak, S. H. Simon, A. Stern, M. Freedman, and S. Das Sarma, Non-Abelian anyons and topological quantum computation, *Rev. Mod. Phys.* **80**, 1083 (2008).

- [10] J. Alicea, New directions in the pursuit of Majorana fermions in solid state systems, *Rep. Prog. Phys.* **75**, 076501 (2012).
- [11] C. Beenakker, Search for Majorana Fermions in Superconductors, *Annu. Rev. Condens. Matter Phys.* **4**, 113 (2013).
- [12] S. Yonezawa, Nematic Superconductivity in Doped  $\text{Bi}_2\text{Se}_3$  Topological Superconductors, *Condens. Matter* **4**, 2 (2018).
- [13] S. Sasaki, Z. Ren, A. A. Taskin, K. Segawa, L. Fu, and Y. Ando, Odd-Parity Pairing and Topological Superconductivity in a Strongly Spin-Orbit Coupled Semiconductor, *Phys. Rev. Lett.* **109**, 217004 (2012).
- [14] M. Novak, S. Sasaki, M. Kriener, K. Segawa, and Y. Ando, Unusual nature of fully gapped superconductivity in In-doped  $\text{SnTe}$ , *Phys. Rev. B* **88**, 140502(R) (2013).
- [15] L. P. He, Z. Zhang, J. Pan, X. C. Hong, S. Y. Zhou, and S. Y. Li, Full superconducting gap in the doped topological crystalline insulator  $\text{Sn}_{0.6}\text{In}_{0.4}\text{Te}$ , *Phys. Rev. B* **88**, 014523 (2013).
- [16] T. Hashimoto, K. Yada, M. Sato, and Y. Tanaka, Surface electronic state of superconducting topological crystalline insulator, *Phys. Rev. B* **92**, 174527 (2015).
- [17] T. Kawakami, T. Okamura, S. Kobayashi, and M. Sato, Topological Crystalline Materials of  $J = 3/2$  Electrons: Antiperovskites, Dirac Points, and High Winding Topological Superconductivity, *Phys. Rev. X* **8**, 041026 (2018).
- [18] S. Kobayashi and M. Sato, Topological Superconductivity in Dirac Semimetals, *Phys. Rev. Lett.* **115**, 187001 (2015).
- [19] B. Lu, K. Yada, M. Sato, and Y. Tanaka, Crossed Surface Flat Bands of Weyl Semimetal Superconductors, *Phys. Rev. Lett.* **114**, 096804 (2015).
- [20] L. Aggarwal, A. Gaurav, G. S. Thakur, Z. Haque, A. K. Ganguli, and G. Sheet, Unconventional superconductivity at mesoscopic point contacts on the 3D Dirac semimetal  $\text{Cd}_3\text{As}_2$ , *Nat. Mater.* **15**, 32 (2016).
- [21] H. Wang, H. Wang, H. Liu, H. Lu, W. Yang, S. Jia, X.-J. Liu, X. Xie, J. Wei, and J. Wang, Observation of superconductivity induced by a point contact on 3D Dirac semimetal  $\text{Cd}_3\text{As}_2$  crystals, *Nat. Mater.* **15**, 38 (2016).
- [22] H. Wang, H. Wang, Y. Chen, J. Luo, Z. Yuan, J. Liu, Y. Wang, S. Jia, X.-J. Liu, J. Wei, and J. Wang, Discovery of tip induced unconventional superconductivity on Weyl semimetal, *Sci. Bulletin* **62**, 425 (2017).
- [23] L. Hao and T. K. Lee, Surface spectral function in the superconducting state of a topological insulator, *Phys. Rev. B* **83**, 134516 (2011).
- [24] T. H. Hsieh and L. Fu, Majorana Fermions and Exotic Surface Andreev Bound States in Topological Superconductors: Application to  $\text{Cu}_x\text{Bi}_2\text{Se}_3$ , *Phys. Rev. Lett.* **108**, 107005 (2012).
- [25] A. Yamakage, K. Yada, M. Sato, and Y. Tanaka, Theory of tunneling conductance and surface-state transition in superconducting topological insulators, *Phys. Rev. B* **85**, 180509(R) (2012).
- [26] A. Yamakage, K. Yada, M. Sato, and Y. Tanaka, Theory of tunneling spectroscopy in a superconducting topological insulator, *Physica C: Superconductivity* **494**, 20 (2013).
- [27] B. J. Wieder, B. Bradlyn, Z. Wang, J. Cano, Y. Kim, H.-S. D. Kim, A. M. Rappe, C. L. Kane, and B. A. Bernevig, Wallpaper fermions and the nonsymmorphic Dirac insulator, *Science* **361**, 246 (2018).
- [28] D.-C. Ryu, J. Kim, H. Choi, and B. I. Min, Wallpaper Dirac Fermion in a Nonsymmorphic Topological Kondo Insulator:  $\text{PuB}_4$ , *J. Am. Chem. Soc.* **142**, 19278 (2020).
- [29] X. Zhou, C.-H. Hsu, C.-Y. Huang, M. Iraola, J. L. Mañes, M. G. Vergniory, H. Lin, and N. Kioussis, Glide symmetry protected higher-order topological insulators from semimetals with butterfly-like nodal lines, *npj Comput. Mater.* **7**, 202 (2021).
- [30] N. Mao, H. Wang, Y. Dai, B. Huang, and C. Niu, Third-order topological insulators with wallpaper fermions in  $\text{Tl}_4\text{PbTe}_3$  and  $\text{Tl}_4\text{SnTe}_3$ , *npj Comput. Mater.* **8**, 154 (2022).
- [31] Y. Hwang, Y. Qian, J. Kang, J. Lee, D. Ryu, H. C. Choi, and B.-J. Yang, Magnetic wallpaper Dirac fermions and topological magnetic Dirac insulators, *npj Comput. Mater.* **9**, 65 (2023).
- [32] K. Mizuno and A. Yamakage, Hall effect of ferro/antiferromagnetic wallpaper fermions, *Phys. Rev. B* **107**, 235301 (2023).
- [33] K. Mizuno and A. Yamakage, Magnon-mediated superconductivity at the interface between a ferromagnetic insulator and a topological crystalline insulator with wallpaper fermions, *Phys. Rev. B* **112**, 035303 (2025).
- [34] K. Yoda and A. Yamakage, Superconducting Gap Structures in Wallpaper Fermion Systems, *J. Low Temp. Phys.* **222**, 44 (2026).
- [35] A. Umerski, Closed-form solutions to surface Green's functions, *Phys. Rev. B* **55**, 5266 (1997).
- [36] M. I. Aroyo, J. M. Perez-Mato, D. Orobengoa, E. Tasci, G. De La Flor, and A. Kirov, Crystallography online: Bilbao crystallographic server, *Bulgarian Chemical Communications* **43**, 183 (2011).
- [37] M. I. Aroyo, J. M. Perez-Mato, C. Capillas, E. Kroumova, S. Ivantchev, G. Madariaga, A. Kirov, and H. Wondratschek, Bilbao Crystallographic Server: I. Databases and crystallographic computing programs, *Zeitschrift für Kristallographie - Crystalline Materials* **221**, 15 (2006).
- [38] M. I. Aroyo, A. Kirov, C. Capillas, J. M. Perez-Mato, and H. Wondratschek, Bilbao Crystallographic Server. II. Representations of crystallographic point groups and space groups, *Acta Cryst. A* **62**, 115 (2006).
- [39] M. I. Aroyo, D. Orobengoa, G. de la Flor, E. S. Tasci, J. M. Perez-Mato, and H. Wondratschek, Brillouin-zone database on the Bilbao Crystallographic Server, *Acta Cryst. A* **70**, 126 (2014).
- [40] K. Satow and A. Yamakage, Symmetry-adapted models for multifold fermions with spin-orbit coupling, *Phys. Rev. B* **112**, 195206 (2025).
- [41] The terms  $H_{\parallel}^{(1)}(\mathbf{k})$ ,  $H_{\parallel}^{(2)}(\mathbf{k})$ ,  $H_{\perp}^{(1)}(\mathbf{k})$ , and  $H_{\perp}^{(3)}(\mathbf{k})$  were derived in Ref. 27.
- [42] M. Sato, Y. Tanaka, K. Yada, and T. Yokoyama, Topology of Andreev bound states with flat dispersion, *Phys. Rev. B* **83**, 224511 (2011).
- [43] Y. Xiong, A. Yamakage, S. Kobayashi, M. Sato, and Y. Tanaka, Anisotropic Magnetic Responses of Topological Crystalline Superconductors, *Crystals* **7**, 58 (2017).
- [44] Y. Yamazaki, S. Kobayashi, and A. Yamakage, Magnetic response of Majorana Kramers pairs with an order-two symmetry, *Phys. Rev. B* **103**, 094508 (2021).
- [45] L. Elcoro, B. J. Wieder, Z. Song, Y. Xu, B. Bradlyn, and B. A. Bernevig, Magnetic topological quantum chemistry, *Nat. Commun.* **12**, 5965 (2021).
- [46] Y. Xu, L. Elcoro, Z.-D. Song, B. J. Wieder, M. G.

- Vergniory, N. Regnault, Y. Chen, C. Felser, and B. A. Bernevig, High-throughput calculations of magnetic topological materials, [Nature](#) **586**, 702 (2020).
- [47] Reference 43 shows that all even-parity pairings have zero magnetic winding numbers.
- [48] J. C. Y. Teo, L. Fu, and C. L. Kane, Surface states and topological invariants in three-dimensional topological insulators: Application to  $\text{Bi}_{1-x}\text{Sb}_x$ , [Phys. Rev. B](#) **78**, 045426 (2008).